Quantifying the leading role of the surface state in the Kondo effect of Co/Ag(111)

M. Moro-Lagares,[1,2,3] J. Fernández,[4] P. Roura-Bas,[4] M. R. Ibarra,[1,5] A. A. Aligia,[4,*] and D. Serrate[1,5,†]

[1]*Instituto de Nanociencia de Aragón, Laboratorio de Microscopias Avanzadas, University of Zaraqoza, E-50018 Zaragoza, Spain*

[2]*Institute of Physics, Academy of Sciences, 18221 Prague, Czech Republic*

[3]*Regional Centre of Advanced Technologies and Materials, Faculty of Science, Department of Physical Chemistry, Palacky University, 78371 Olomouc, Czech Republic*

[4]*Centro Atómico Bariloche and Instituto Balseiro, Comisión Nacional de Energía Atómica, 8400 Bariloche, Argentina*

[5]*Departamento Física Materia Condensada, University of Zaraqoza, E-50018 Zaragoza, Spain*

(Received 6 March 2018; revised manuscript received 31 May 2018; published 26 June 2018)

Using a combination of scanning tunneling spectroscopy and atomic lateral manipulation, we obtained a systematic variation of the Kondo temperature T_K of Co atoms on Ag(111) as a function of the surface-state contribution to the total density of states at the atom adsorption site ρ_s. By sampling the T_K of a Co atom on positions where ρ_s was spatially resolved beforehand, we obtain a nearly linear relationship between the magnitudes. We interpret the data on the basis of an Anderson model including orbital and spin degrees of freedom [SU(4)] in good agreement with the experimental findings. The fact that the onset of the surface band is near the Fermi level is crucial to finding the observed linear behavior. In light of this model, the quantitative analysis of the experimental data evidences that at least a quarter of the coupling of Co impurities with extended states takes place through the hybridization to surface states. This result is of fundamental relevance in the understanding of Kondo screening of magnetic impurities on noble-metal surfaces, where bulk and surface electronic states coexist.

DOI: 10.1103/PhysRevB.97.235442

I. INTRODUCTION

Single atoms with partially filled d or f shells on a solid-state surface are known to exhibit strong electron correlations leading to a wide range of physical ground states. The magnetic properties of such impurities on metals are inherently connected with many-body interactions between the localized magnetic moment and the conduction electrons [1–9]. In this framework, the Kondo effect [1,10,11] is the one most frequently found. Since this phenomenon is an archetypal example of the formation of a many-body quantum state, it is central to the understanding of the electronic behavior of complex strongly correlated electrons systems such as heavy fermions [11,12], Kondo insulators [13], and nanoscale systems [2,3,5,14–27].

Thanks to the large spatial and energy resolution of scanning tunneling microscopy (STM) and spectroscopy (STS) [2,18,19], these tools are extremely well suited to accessing the spectroscopic features of adsorbate-induced many-body resonances in tunneling differential conductance (dI/dV). Most STM studies on Kondo impurities are performed on noble-metal (111) surfaces, where bulk and surface electrons coexist [2,3,5,19–28]. Unavoidably, the question of whether surface or bulk electrons play the leading role in the Kondo effect arises. To date, the answer remains unclear because there are conflicting conclusions depending on the technical approach to the problem. Since bulk electrons decay much faster than surface-state electrons into the crystal, it has been common practice to measure the Kondo resonance as a function of the lateral distance to the atom [3,5,29,30].

For instance, Henzl and Morgenstern [5] concluded that bulk electrons determine the Kondo temperature T_K of Co/Ag(111) by intentionally depleting the spectral weight of the surface state at the Fermi level. The study of the Kondo resonance next to a monoatomic step edge led to the conclusion that the role of the surface states is marginal [21]. This is supported by the weak dependence of T_K of Co on noble-metal surfaces [31] with marked differences in the weight of their surface states relative to the bulk ones. On the contrary, the theoretically predicted [29,30] oscillations of the resonance line shape as a function of the tip lateral displacement on the order of the bulk electrons' Fermi wavelength have not been observed [2,3,5]. In fact, the theoretical description by Merino *et al.* [32] cannot explain the distance-dependent data for Co/Cu(111) [3] without a major involvement of the surface states.

The seminal work on the quantum mirage of the Kondo resonance in the focus of elliptical resonators proves unambiguously a finite contribution of surfaces states [20]. Based on the relative intensity of dI/dV at both foci (one with a Co impurity and the other empty), a lower bound of $1/10$ for the relative contribution of surface states has been estimated [33]. Moreover, the rather high $T_K \sim 180$ K of a Co porphyrin on $(\sqrt{3} \times \sqrt{3})$Ag-Si(111), where bulk electron states are not present, indicates that a significant coupling between the surface states and magnetic impurity is possible [34]. In support of this, it was recently shown that dI/dV of Ag(111) oscillates as the resonance width of Co atoms near

*aligia@cab.cnea.gov.ar
†serrate@unizar.es

step edges, quantum resonators, or another atom [35]. It is worth noting that, from the theoretical point of view, the Kondo effect is extremely sensitive to the hybridization channels between the impurity and the metal host electrons, which exhibit nontrivial dependencies on the k-space electronic structure of the surface and the actual adsorption geometry [36]. Thus, direct comparison of the Kondo resonance among different environments of the same adatom is physically inaccurate.

In this paper, we quantify the role of surface electron states in the Kondo effect of Co adatoms on Ag(111). We characterize their Kondo spectral features while varying just one single parameter of the problem: the surface-state contribution to the local density of states of the substrate ρ_s. In Secs. II and III we develop the theoretical background on the basis of an Anderson model with SU(4) symmetry, which is consistent with the experimental spectroscopy as opposed to the SU(2) one [35]. Section IV is devoted to the experimental differential conductance dI/dV at position $\mathbf{R}$ with (G_K) and without (G) Co impurity between the tip and the Ag(111) surface. The analysis of $T_K(\mathbf{R})$ and the amplitude of the Kondo resonance reveals that both magnitudes increase monotonically with $G(\mathbf{R})$. The theoretical calculation of the energy-resolved G for varying ρ_s is given in Sec. V, using both the noncrossing approximation (NCA) and poor man's scaling (PMS). Finally, in Sec. VI the experimental and theoretical physical parameters are compared. We show that the coupling of the Co impurity state with extended states stemming from the surface state could be the dominant one and prove a threshold of at least one fourth of that of the bulk states.

II. SYMMETRY ANALYSIS

In analogy with other noble-metal surfaces [37], the Co atoms might occupy two inequivalent hollow positions on the Ag(111) surface, depending on whether the Co atoms lie above a Ag atom of the second layer or not (fcc/hcp). In both cases the symmetry point group is C_{3v}. This group has three irreducible representations: A_1 and A_2 of dimension one and the two-dimensional representation E. Disregarding spin for the moment, the Co $3d$ orbitals are split into one A_1 singlet and two E doublets, as sketched on the left side of Fig. 1. Choosing the coordinates in such a way that z is perpendicular to the surface and one of the Ag atoms nearest Co lies in the xz plane,

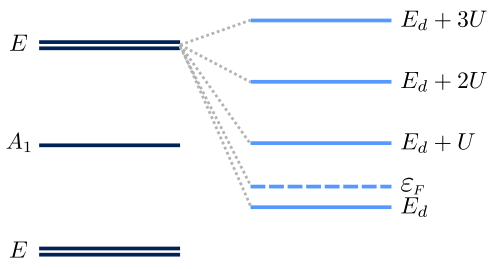

FIG. 1. Left: scheme of the splitting of the (one-particle) $3d$ orbitals under the point group C_{3v}. Right: scheme of the splitting of the four antibonding states of symmetry E by the Coulomb repulsion. ε_F denotes the position of the Fermi energy compatible with the position of the observed Fano antiresonance.

the $3d$ orbital with symmetry $3z^2 - r^2$ transforms as the A_1 representation, xz and yz transform like the E representation, and $x^2 - y^2$ ($-xy$) transforms under the operations of C_{3v} in the same way as xz (yz). Any Hamiltonian that respects the point group symmetry (without additional symmetry) mixes these two doublets, leading to bonding and antibonding states. In particular, the antibonding E states have the form

$$|e_1\rangle = \alpha|xz\rangle + \beta|(x^2 - y^2)/2\rangle,$$
$$|e_2\rangle = \alpha|yz\rangle - \beta|xy\rangle. \quad (1)$$

Additional adatoms on the surface break the C_{3v} symmetry, but this effect is small if these atoms are sufficiently far from the Co atom under study, as is the case in this work.

The Coulomb repulsion inside the $3d$ orbitals splits the energy necessary to add electrons in the same orbital. For example, let us call E_d the energy necessary to add the first electron in one of the antibonding E orbitals with any spin. This energy does not depend on the particular antibonding orbital chosen (e_1 or e_2) or its spin. However, the extra energy cost to add the second electron is the Coulomb repulsion U between them. Similarly, the necessary energy to add the third or fourth electron is E_d plus the Coulomb repulsion with the previous ones. This is presented schematically on the right of Fig. 1. The actual position of the levels is more complex because it is modified by exchange and pair-hopping terms (see, for example, Ref. [38]), but they do not affect our treatment. For example, the ground state for occupancy 2 in the antibonding E is a triplet due to Hund's rules. Instead, for occupancy 3 of theses state the ground state is degenerate and is formed by two spin doublets with one hole in either e_1 or e_2. A similar splitting takes place for the bonding E and the A_1 states, which remain occupied in the neutral Co atom.

While symmetry alone cannot determine the ordering of the levels, the position of the observed Fano-Kondo dip ω_K for positive energies of the order of the Kondo temperature T_K or larger [see, for instance, Fig. 2(b)] [39] points to an SU(4) Kondo system with occupancy close to 1, as we show below. This is consistent with the configuration $3d^7$ expected for a neutral Co atom, with four electrons occupying the bonding E orbitals, two in the A_1 orbital, and the remaining electron in one antibonding E orbital (Fig. 1). Other possibilities can be disregarded. For example, if both A_1 states were the highest in energy, putting two holes there and one in the antibonding E orbitals, the model presented in Sec. III still holds after an electron-hole transformation in the antibonding E orbitals, in which case the Kondo dip would be to the left of the Fermi energy (i.e., same differential conductance as in Fig. 2(b) but with the opposite bias sign). Assuming a $3d^8$ configuration, one has two possibilities to obtain a Kondo state: (i) two holes in the antibonding E states, except in this case the Kondo dip would be centered at the Fermi level [40], or (ii) one hole in an E state and one hole in an A_1 state. This is the case of Fe phthalocyanine on Au(111), which shows a two-stage Kondo effect with two features with different widths at the Fermi energy [25], completely different from our case. We have not discussed above combinations of holes in bonding and antibonding E orbitals because they are unlikely for Co.

Therefore, two channels are necessary to describe the system, and one-channel models [like the ordinary one-channel

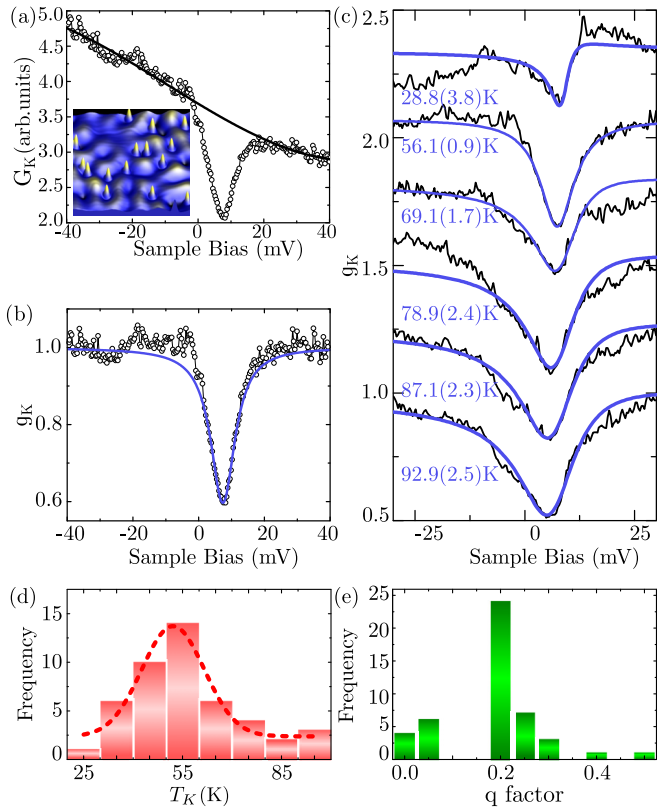

FIG. 2. (a) Representative raw dI/dV [$G_K(V)$, open circles] showing the Kondo zero-bias feature at the center of a single Co atom and background estimation [$\mathcal{G}_0(V)$, solid line]. (b) Fit of the resulting $g_K(V)$ to Eq. (7), yielding $T_K = 56.1 \pm 0.9$ K, $q = 0$, and $\omega_K = 7.39 \pm 0.04$ meV. (c) Dispersion found in the Kondo resonance of a set of atoms spread on Ag(111) with the corresponding fit and T_K value. (d) Kondo temperature and (e) q factor statistics. Using a Gaussian distribution profile (dashed line) for the T_K histogram, we obtain $\langle T_K \rangle = 52.1 \pm 9.4$ K.

SU(2) Anderson or Kondo model] are ruled out. One has, in principle, a spin SU(2) times orbital SU(2) model. However, for large U (we take $U \to \infty$, but this is not an essential approximation [41]) the symmetry is SU(4) [larger than SU(2) × SU(2)], including orbital and spin degeneracies.

III. MODEL AND FORMALISM

A. Hamiltonian

The Hamiltonian can be written as

$$H = \sum_{ki\sigma} \varepsilon_k^s s_{ki\sigma}^\dagger s_{ki\sigma} + \sum_{k\sigma} \varepsilon_k^b b_{ki\sigma}^\dagger b_{ki\sigma} + E_d \sum_\sigma d_{i\sigma}^\dagger d_{i\sigma} + U \sum_{i\sigma \neq j\sigma'} d_{i\sigma}^\dagger d_{i\sigma} d_{j\sigma'}^\dagger d_{j\sigma'} + \sum_{k\sigma} V_k^s [d_{i\sigma}^\dagger s_{ki\sigma} + \text{H.c.}] + \sum_{k\sigma} V_k^b [d_{i\sigma}^\dagger b_{ki\sigma} + \text{H.c.}], \quad (2)$$

where $d_{i\sigma}^\dagger$ creates an electron in the antibonding orbital $|e_i\rangle$ with spin σ and $s_{ki\sigma}^\dagger$ ($b_{ki\sigma}^\dagger$) are creation operators for an electron in the kth surface (bulk) conduction eigenstate with symmetry i and spin σ.

We assume constant densities of bulk states ρ_b extending in a wide range from $-D$ to D and ρ_s extending from D_s to D ($|D_s| < D$). As we shall show, the fact that the surface band begins abruptly near the Fermi level at $D_s = -67$ meV [42] (neglected in alternative treatments [35]) plays an essential role in the interpretation of the results. We also assume constant hybridizations $V_b = V_k^b$ and $V_s = V_k^s$. We believe that these assumptions are not crucial as long as the dependence of these parameters on energy is smooth in a range of a few times T_K around the Fermi energy. We define the couplings of the impurity state to bulk and surface state electrons as $\Delta_b = \pi \rho_b |V_k^b|^2$ and $\Delta_s = \pi \rho_s |V_k^s|^2$, respectively. Our work allows us to experimentally determine the ratio of these two quantities. E_d is the energy of the relevant impurity state.

We solve the model using two techniques: NCA (Sec. V A) [11,43] and PMS (Sec. V B) [11,44] on the effective Coqblin-Schrieffer model. These approaches are known to reproduce correctly the relevant energy scale T_K and its dependence on the Anderson parameters. In contrast to the numerical renormalization group in which the logarithmic discretization of the conduction band [45,46] broadens finite-energy features [46,47] and leads to inaccurate Kondo temperatures when a step in the conduction band is near the Fermi level, NCA correctly describes these features. For instance, the intensity and the width of the charge-transfer peak of the spectral density (the one near E_d) were found [48,49] to be in agreement with other theoretical methods [49–51] and experiment [52]. The NCA works satisfactorily in cases in which the density of conduction states is not smooth [53], including, in particular, a step in the conduction band [54]. Furthermore, it has a natural extension to nonequilibrium conditions [55], and it is especially suitable for describing satellite peaks of the Kondo resonance, such as those observed in Ce systems [56,57], or away from zero-bias voltage in nonequilibrium transport [58–61]. Due to shortcomings of the approximation for finite U [50,62,63], we restrict our calculations to $U \to \infty$, but this is not an essential approximation in our case [41].

The PMS is a perturbative approach that progressively integrates out a small portion of the conduction states lying at the bottom and top of the conduction bands, renormalizing the Kondo exchange coupling J_K [11,44].

B. The STM tunneling conductance

The differential conductance dI/dV is proportional to the spectral density of the mixed state $h_{i\sigma}(\mathbf{R}_t)$ at the position of the STM tip $\mathbf{R}_t$ [33]:

$$G_K(eV) = dI/dV \propto \sum_{i\sigma} \rho_{hi\sigma}(eV),$$

$$\rho_{hi\sigma}(\omega) = \frac{1}{2\pi j}[\tilde{G}_{hi\sigma}(\omega - j\epsilon) - \tilde{G}_{hi\sigma}(\omega + j\epsilon)],$$

$$h_{i\sigma}(\mathbf{R}_t) = \frac{1}{N}[s_{i\sigma}(\mathbf{R}_t) + p_b b_{i\sigma}(\mathbf{R}_t) + p_d d_{i\sigma}(\mathbf{R}_t)], \quad (3)$$

where V is the sample bias potential of the STM, e is the electron elementary charge, $\tilde{G}_{hi\sigma}(\omega) = \langle\langle h_{i\sigma}; h_{i\sigma}^\dagger \rangle\rangle_\omega$ is the Green's function of $h_{i\sigma}(\mathbf{R}_t)$, j is the imaginary unit, ϵ is a positive infinitesimal, N is a normalization factor, p_b is the ratio of the tunneling matrix element between the STM tip and the

bulk states $b_{i\sigma}$ and between the tip and surface states $s_{i\sigma}$, and p_d is the analogous ratio for Co state $d_{i\sigma}(\mathbf{R}_t)$ and surface states at the tip position. $h_{i\sigma}(\mathbf{R}_t)$ represents the linear combination of surface, bulk, and Co $3d$ states probed by the tip.

Using equations of motion, $\rho_{hi\sigma}(\omega)$ can be related to the Green's function for the d electrons $\tilde{G}_{di\sigma}(\omega) = \langle\langle d_{i\sigma}; d^{\dagger}_{i\sigma}\rangle\rangle_{\omega}$ and the unperturbed Green's functions for conduction/bulk electrons $\tilde{G}^0_{s/b}(\omega)$. In the absence of magnetic and symmetry-breaking fields we can drop the subscripts $i\sigma$:

$$\tilde{G}_h(\omega) = \tilde{G}^0_s(\omega) + p_b^2\tilde{G}^0_b(\omega) + \Delta\tilde{G}_h(\omega). \tag{4}$$

$\Delta\tilde{G}_h(\omega) = 0$ if the Co impurity is absent, and if not,

$$\begin{aligned}\Delta\tilde{G}_h(\omega) &= F^2(\omega)\tilde{G}_d(\omega),\\ F(\omega) &= V_s\tilde{G}^0_s(\omega) + p_bV_b\tilde{G}^0_b(\omega) + p_d,\end{aligned} \tag{5}$$

where

$$\begin{aligned}\tilde{G}^0_b(R_i,R_i,\omega) &= \rho_b\left[\ln\left(\frac{\omega+D}{\omega-D,}\right)\right],\\ \tilde{G}^0_s(R_i,R_i,\omega) &= \rho_s\left[\ln\left(\frac{\omega-D_s}{\omega-D}\right)\right].\end{aligned} \tag{6}$$

IV. EXPERIMENTAL RESULTS

Single Co atoms were deposited at low temperatures onto the Ag(111) surface ($T_{ev} \sim 3$ K for an experimental temperature $T = 1.1$ K) cleaned by repeated cycles of sputtering with Ar^+ and annealing at 500 °C in UHV ($P_{\text{base}} \leqslant 1\times10^{-10}$ mbar). We use a lock-in amplifier to perform STS as a function of the applied sample bias V. STS was acquired at constant height defined by the regulation set point V_0, I_0 on Ag(111) with rms modulation voltage V_{mod} and implemented in two modes: (i) single-point dI/dV spectroscopy ($V_{\text{mod}} = 0.5$ mV, $V_0 = -100$ mV, $I_0 = 42$ pA) on top of Co atoms to obtain the energy-resolved $G_K(\mathbf{R})$ and (ii) $dI/dV(x,y)$ mapping at the Fermi level ($V_{\text{mod}} = 1$ mV, $V_0 = -100$ mV, $I_0 = 200$ pA) to measure the spatially resolved $G(\mathbf{R})$ of the Ag(111) inspected area after clearing it away from atoms by means of atomic manipulation (the typical set point for manipulation is $V_0 = 3$ mV, $I_0 = 40$–70 nA). The working temperature is $T = 1.1$ K or $T = 4.7$ K, with the Kondo features of one atom in STS being identical at both temperatures.

Experimentally, the Kondo effect of isolated Co atoms on metals manifests as a Fano resonance [2,19,31,64] in the impurity G_K near the Fermi level. We describe this singularity as $G_K = \mathcal{G}_0 g_K$, where $\mathcal{G}_0(\mathbf{R},\omega)$ is the convolution of the tip and the impurity density of states in the absence of Kondo screening and $g_K(\mathbf{R},\omega)$ contains the Fano function $\mathcal{F}(x,q) = (x+q)^2/1+x^2$ as follows:

$$g_K(\mathbf{R},\omega) = [1 - A_K(\mathbf{R})] + A_K(\mathbf{R})\mathcal{F}\left[\frac{\omega-\omega_K}{\Gamma_0(\mathbf{R})/2},q\right]. \tag{7}$$

Here $\omega = eV$, ω_K is the energy of the center of the Kondo resonance, q is the Fano asymmetry factor, $A_K(\mathbf{R})$ is the resonance amplitude when the atom sits at surface position $\mathbf{R}$, and $\Gamma_0(\mathbf{R})$ is the resonance width, which is related to the Kondo temperature as $2k_B T_K \simeq \Gamma_0$ for $T/T_K \to 0$ [19,65]. Below T_K the spin of the extended states couples antiferromagnetically and screens the impurity spin, giving rise to the Kondo

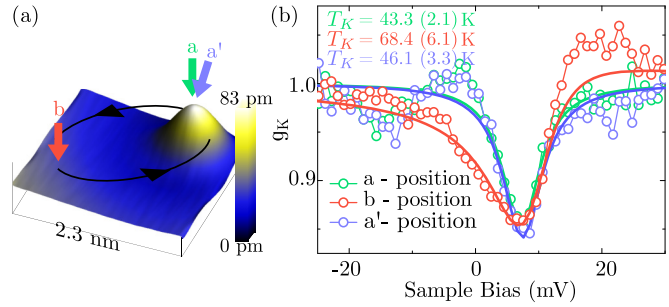

FIG. 3. (a) Representation of the experiment carried out in the study of the variations of the Kondo resonance with the point contact ρ_s. (b) The dI/dV spectrum (circles) and fit to Eq. (7) of the Co atom at the a position (green), b position (red), and a' position (blue). The a' position is the same as the a position after atomic manipulation.

state [10,11]. Figures 2(a) and 2(b) show the analysis of a Kondo resonance based on Eq. (7), which permits us to extract the parameters $T_K(\mathbf{R})$, $A_K(\mathbf{R})$, q, and ω_K for each individual atom at position $\mathbf{R}$.

We first analyze G_K of several Co atoms dispersed over the surface at their position right after the evaporation process (i.e., prior to any atom repositioning with the tip). Figures 2(c)–2(e) unveil a significant uncertainty in the parameters describing the Kondo resonance. The histograms elaborated from a set of 40 different atoms are shown in Figs. 2(d) and 2(e). T_K spans over a range of 28 K $\leqslant T_K \leqslant$ 95 K, with $\langle T_K\rangle = 52.1 \pm 9.4$ K being the most probable value. The most frequently found value for A_K and q is 0.2.

Apart from the hcp/fcc character of the hollow sites in a (111) surface termination, the adsorption geometry of disperse Co atoms is indistinguishable. We have confirmed that the Kondo parameters are the same in both sites except for a slightly lower amplitude A_K in one of them. Therefore, the different values obtained for T_K and q suggest a sensitivity to the density of surface states $\rho_s(\mathbf{R})$. Particularly, in Ag(111), the onset of the surface state lies in close proximity ($D_s = -67$ meV) to the Fermi level [42], leading to a Fermi wavelength $\lambda_F \sim 8$ nm [28], which is comparable to the distance between surface scatterers such as step edges, point impurities, and Co adatoms. This will produce interference patterns in $\rho_s(\mathbf{R})$ with a characteristic length scale of $\lambda_F/2$. We have shown elsewhere [28] that ρ_s contributes strongly to the total density of states $h_{i\sigma}(\mathbf{R}_t)$ (ρ_h) probed by the tip. Therefore, it is natural to expect that changes in $\rho_s(\mathbf{R})$ will lead to the observed dispersion of T_K of Co/Ag(111), through the hybridization of the Co $3d$ electrons with the surface states. This will become clear in Sec. V B, where an analytical expression for the dependence of T_K on ρ_s is presented.

To benchmark the correlation of T_K with the electronic properties of the substrate, we measure g_K [see Eq. (7)] over a Co atom at its natural adsorption site $\mathbf{R}$ and subsequently at another position $\mathbf{R}'$ far enough to have presumably a different ρ_s ($|\mathbf{R}-\mathbf{R}'| \sim \lambda_F/2$). In Fig. 3 we show g_K at each site in the absence of any tip change during the manipulation procedure. We find a strong variation of $\Delta T_K = T_K(\mathbf{R}') - T_K(\mathbf{R}) = 24 \pm 4$ K, well above the experimental uncertainty. This experiment shows unambiguously that the coupling strength between the localized spin and the Fermi gas of conduction

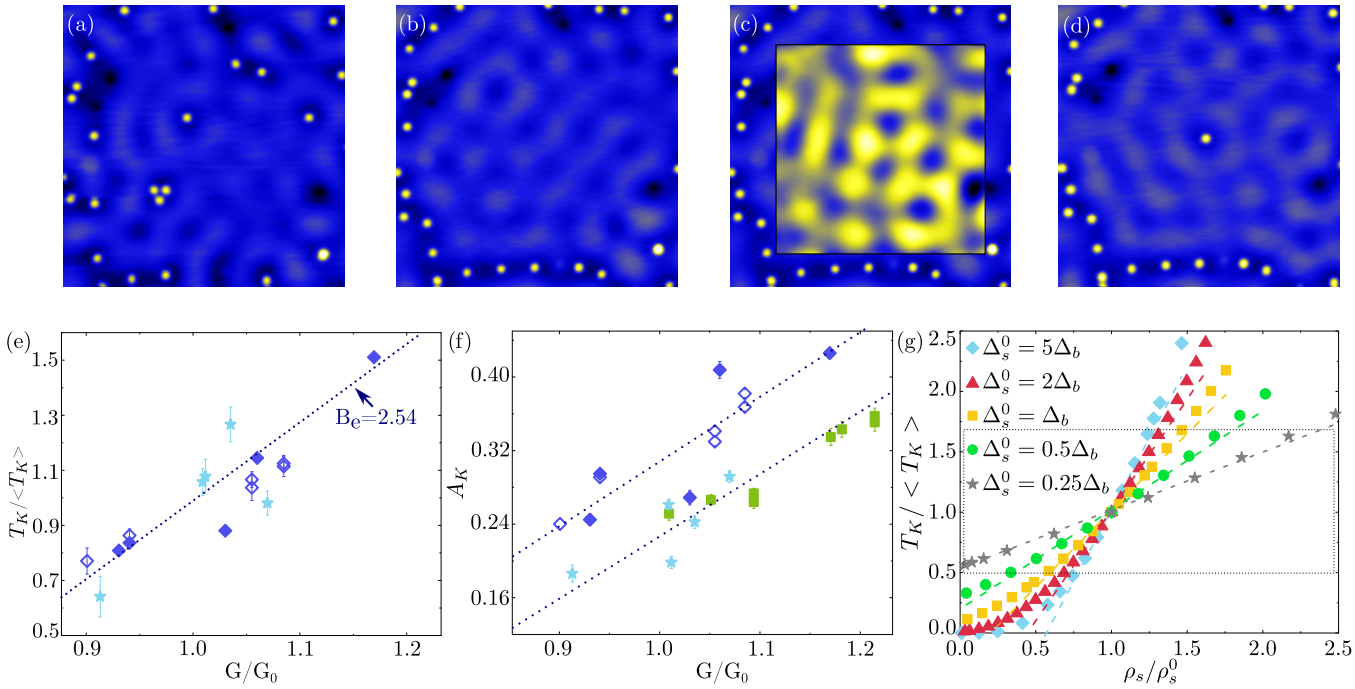

FIG. 4. T_K and A_K variations with $G(\mathbf{R})$. (a) STM image of Co/Ag(111) after Co deposition. (b) Co atoms are removed from the working area to avoid their influence on G. (c) Inset: constant-height $G(\mathbf{R}) = dI/dV$ map taken at $V = 3$ mV ($I_0 = 200$ pA, $V_0 = -100$ mV, and $V_{\text{mod}} = 1$ mV). (d) Co atom relocated at a certain position over the surface. (e) Experimental dependence of $T_K/\langle T_K\rangle$ on the normalized local tunneling conductance G/G_0. (f) Experimental dependence of A_K on G/G_0. In (e) and (f), the color code represents data sets taken with the same tip, while for the same color, the open and solid diamonds distinguish data sets at two different close working areas. All measurements were taken in constant-height mode at $T = 1.1$ K ($I_0 = 42$ pA, $V_0 = -100$ mV, and $V_{\text{mod}} = 0.5$ mV). (g) Theoretical dependence of $T_K/\langle T_K\rangle$ on ρ_s/ρ_s^0 for different values of Δ_s^0/Δ_b. The dashed lines are linear fits in the region $0.5 < T_K/\langle T_K\rangle < 1.5$. The region enclosed within the dotted rectangle corresponds to the experimental parameter range.

electrons is strongly influenced by the local value of ρ_s at each contact point.

Next, we evaluate more precisely this position-dependent Kondo effect through the analysis of T_K and A_K of Co atoms relocated in a region where $G(\mathbf{R})$ at Fermi level has previously been characterized (without Co atoms) in constant-height conditions. First, we clean out the atoms in the selected working area, as depicted in Figs. 4(a) and 4(b). Second, we take a $G(\mathbf{R})$ image of the differential conductance near the Fermi level ($0 < V < 3$ mV), as shown in Fig. 4(c), whose maxima and minima reflect the characteristic interference pattern of the surface state. Afterwards, a single Co atom is moved across the inspected Ag(111) area [Fig. 4(d)], and we measure its energy spectrum $G_K(\mathbf{R})$ for each $\mathbf{R}$ location. Note that this procedure is free of feedback artifacts and that the drift between consecutive images is corrected by always referring $\mathbf{R}$ to a reference feature of the same image.

At the tip-sample distance at which the experiment is performed, the STM does not exhibit atomic resolution. Thus, $G(\mathbf{R})$ oscillations are contributed by only $\rho_s(\mathbf{R})$, owing to the interference pattern of scattered surface-state quasiparticles. In Figs. 4(e) and 4(f) we plot $T_K/\langle T_K\rangle$ and A_K as a function of G/G_0 for four different data sets gathered together, taken with different tips (symbols) at different working areas (color code). G_0 is defined as the tunneling conductance of an ideal surface without scattering sources. Experimentally, we determine G_0 to be the average differential conductance at Fermi level of a region much larger than λ_F, such as the one shown in Fig. 4(c). This normalization makes the analysis insensitive to the specific electronic structure of the tips used for the experiment. The resulting graphs display a monotonic increase of T_K and A_K with G, which implicitly provides evidence of the linear dependence of these parameters on ρ_s within the experimental boundaries.

V. THEORETICAL RESULTS

In this section we present the theoretical results for the dependence of T_K on the surface-state density ρ_s. For simplicity, from now on we choose the origin of energies to be $\varepsilon_F = 0$. We have taken $D_s = -67$ meV from experiment [21,28,66] and have chosen $D = 4$ eV, $\rho_b = 0.135\,\text{eV}^{-1}$, $\rho_s = 0.0446\ \text{eV}^{-1}$ [28]. The results are rather insensitive to these parameters if the hybridizations are changed to fix the values of Δ_b and Δ_s. For the energy of the occupied antibonding E state with majority spin (see Fig. 1), we take $|E_d| \gg \Delta_{s,b}$ (in particular, $E_d = -2.2$). A different value would simply require a rescaling of $\Delta_{s,b}$.

Concerning the parameters entering Eq. (3), a previous comparison between experiment and theory on the action of Co resonators on the surface states [28] suggests that $p_b^2 \approx 1/16$. At first we took $|p_b| = 1/4$, but this implies a very large surface contribution ($\Delta_s^0/\Delta_b > 6$; see below). Furthermore, this estimation applies to a different tunneling barrier height [28], which may strongly alter the ratio p_b. Therefore, we think that it is better to be cautious and treat p_b as an unknown parameter.

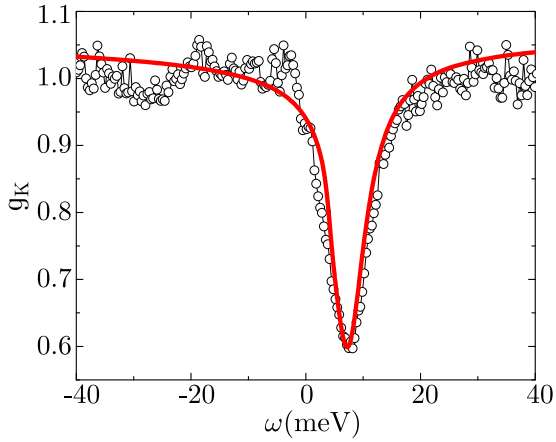

FIG. 5. Differential conductance as a function of voltage. Open circles: experimental g_k [the same as Fig. 2(b)] without background. Red line: theory for $\Delta_s = 69.26$ meV, $\Delta_b = 256.5$ meV, $p_b = 1.16$, and $p_d = 7$.

The shape of the resulting differential conductance dI/dV is rather insensitive to the sign of p_b, but the intensity is smaller for $p_b < 0$. The parameter p_d is determined by fitting the line shape. The line shape is rather insensitive to p_b if p_d is adjusted.

A. Noncrossing approximation

1. Calculation of the Kondo temperature

To determine theoretically the value of the Kondo temperature T_K, we calculate the conductance through the magnetic impurity as a function of temperature $G_d(T)$ for a hypothetical case with $p_d \to \infty$ and look for the temperature such that $G_d(T_K) = \gamma_0/2$, where γ_0 is the ideal conductance of the system (reached for $T = 0$ and occupancy 1 of the impurity level). Alternative definitions of T_K differ in the factor of the order of 1 [67], which is not relevant to us, as we shall show. We are interested in the dependence of T_K with Δ_s. In practice we take

$$G_d(T) = \gamma_0 \frac{\pi \Delta}{2} \int d\omega \left(-\frac{\partial f(\omega)}{\partial \omega}\right) \rho_d(\omega), \tag{8}$$

where $\Delta = \Delta_b + \Delta_s$, $\rho_d(\omega) = \sum_{i\sigma} \rho_{di\sigma}(\omega)$ is the total impurity spectral density adding both orbitals i and spins σ and $f(\omega)$ is the Fermi function.

2. Fit of the experimental data

In Fig. 5 we show one experimental result for the differential conductance for which the resulting T_K is very close to the average one $\langle T_K \rangle$ and the corresponding theoretical fit obtained at the experimental temperature $T = 4.7$ K. For the latter, we have assumed $\Delta_s = 0.27\Delta_b$, $p_b = 1.16$, which is consistent with the experimental slope of T_K vs the tunneling conductance (see below) and adjusted p_d to fit the experimental data. Very similar fits are obtained for larger values of p_b. The fit requires shifting the theoretical results by 4 meV to reach the experimental position of the dip $\omega_K = 7.7$ meV. The reason for this discrepancy might be due to details of the energy dependence of Δ_s, which is particularly sensitive to the position of the adatoms [28] and which we have neglected in our approach.

TABLE I. Slope of $T_K/\langle T_K \rangle$ vs ρ_s/ρ_s^0, the corresponding C_b value (see Sec. VI), and the coefficient of the bulk density of states in Eq. (5) for different ratios $R = \Delta_s^0/\Delta_b$.

R	B	C_b	p_b
0.25	0.480	4.289	1.190
0.27	0.503	4.045	1.156
0.5	0.820	2.098	0.832
1	1.269	1.001	0.575
2	1.835	0.384	0.356
5	2.375	0.070	0.152

Note that for the parameters in Fig. 5, the total width of the Fano dip is $\Gamma_0 = 8.71$ meV, while 2 times T_K obtained from the definition based on Eq. (8) gives $2k_B T_K = 9.78$ meV. This ratio is approximately constant for the different parameters used here. Our Fano fit for this experimental curve gives $T_K = 56.1$ K $\sim$4.83 meV. Therefore, we assume that this value is representative of the average Kondo temperature $\langle T_K \rangle$ observed in experiment. Note that the ratio $T_K/\langle T_K \rangle$ does not depend on the definition of T_K. We define ρ_s^0 and $\Delta_s^0 = \pi \rho_s^0 V_s^2$ as the values of the surface spectral density and Δ_s that lead to $T_K = \langle T_K \rangle$. T_K depends mainly on $\Delta_s + \Delta_b$, and several ratios Δ_s/Δ_b can lead to the same T_K.

In Fig. 4(g) we show the dependence of $T_K/\langle T_K \rangle$ on $\Delta_s/\Delta_s^0 = \rho_s/\rho_s^0$ for several values of $R = \Delta_s^0/\Delta_b$. In good agreement with the experimental behavior of T_K [Fig. 4(e)], we obtain a linear trend in the interval $0.5 < T_K/\langle T_K \rangle < 1.5$ with slope B. As expected, B increases with increasing $R = \Delta_s^0/\Delta_b$. For larger R the linear dependence weakens, and some curvature appears. The results for the slope B for different ratios $R = \Delta_s^0/\Delta_b$ and the corresponding values of p_b are listed in Table I.

B. Poor man's scaling

The PMS [11,44] for this SU(4) problem [or, in general, for SU(N) symmetry] up to second order in the Coqblin-Schrieffer interaction J_K has the same form as for the SU(2) Kondo Hamiltonian treated previously [54], taking NJ_K as the interaction constant. Then, borrowing previous results and taking the limit $U \to \infty$, we obtain the following analytical formula for the Kondo temperature as a function of Δ_b and Δ_s:

$$T_K \simeq A|D_s|^\eta D^{1-\eta} \exp\left[\frac{\pi E_d}{4(\Delta_b + \Delta_s)}\right],$$
$$\eta = \frac{\Delta_s}{(\Delta_b + \Delta_s)}, \tag{9}$$

where for second order in J_K, $A = 1$. Higher-order corrections reduce A and introduce logarithmic corrections. However, in our case, it is not possible to obtain an analytical formula like Eq. (9) if these corrections are included.

In Fig. 6 we plot this function for the same parameters as in Fig. 4(g), showing again a linear dependence in the relevant range of parameters, in agreement with experiment. We obtain

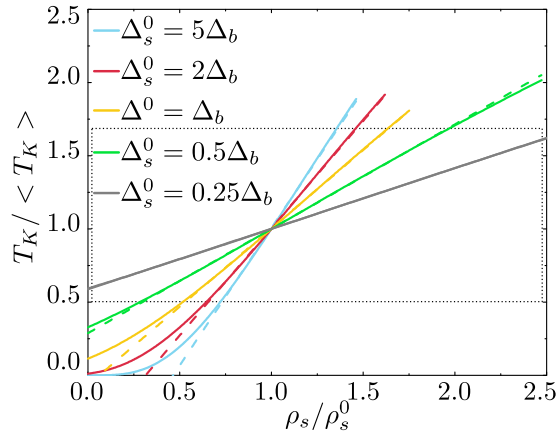

FIG. 6. Same as Fig. 4(g) using Eq. (9). T_K^0 is the value obtained for the same parameters as before and differs from the value of $\langle T_K\rangle$ by a factor of ∼2. The region enclosed within the dotted rectangle corresponds to the experimental parameter range.

a semiquantitative agreement with the NCA (which assumes $U \to \infty$).

Equation (9) sheds light on the expected dependence of T_K as a function of Δ_s. In the experimentally relevant range of parameters the last (exponential) factor has a marked upward curvature which is largely compensated by the factor $|D_s|^\eta D^{1-\eta}$, leading to the approximately linear dependence displayed in Fig. 6. Replacing $|D_s|^\eta D^{1-\eta}$ by $D \sim 4$ eV (as in Ref. [35]) cannot reproduce our experimental results.

In Table II we display the slope B obtained from a linear fit in the interval $0.5 < T_K/\langle T_K\rangle < 1.5$. The slope with NCA is about 13% (for lower R) to 20% (for larger R) larger than that with PMS (compare Tables I and II). The agreement might be improved by including numerically logarithmic corrections of order J_K^3, but we failed in the attempt to calculate them.

VI. QUANTITATIVE DISCUSSION

We have obtained experimentally and theoretically a linear trend of $T_K(\rho_s)$. This might be surprising at first glance since an exponential dependence of T_K on the coupling strength is expected [1,68]. However, due to the always existing bulk contribution, the proximity of the bottom of the surface band to the Fermi level, and the particular region of interest of the parameter phase space [see the analytical PMS result in Eq. (9)], the expected upward curvature is strongly reduced, particularly for small R.

Since the measurements are performed at constant height, the experimental dI/dV without a Co impurity can be written for all positions as $G = C(\rho_s + p_b^2\rho_b)$ [from Eqs. (3) and (4) with $\Delta\tilde{G}_h(\omega) = 0$]. Here C and ρ_b are constants. We write the differential conductance in the form $G = C\rho_s^0(\rho_s/\rho_s^0 + C_b)$, where $C_b = p_b^2\rho_b/\rho_s^0$ is the relative weight of the bulk states in the tunneling conductance at reference point $T_K/\langle T_K\rangle = 1$. C_b is also a constant. Now, the theoretical analog of G_0 yields $G_0 = C\rho_s^0(1 + C_b)$.

TABLE II. Same as Table I calculated with PMS.

R	B	C_b	p_b
0.25	0.414	5.135	1.302
0.27	0.445	4.709	1.247
0.5	0.713	2.562	0.920
1	1.070	1.374	0.674
2	1.465	0.734	0.492
5	1.878	0.352	0.341

To compare the values of our theoretical slope B of $T_K/\langle T_K\rangle$ vs ρ_s/ρ_s^0 with the experimental slope $B_e \simeq 2.54$ of $T_K/\langle T_K\rangle$ vs G/G_0 obtained from the data in Fig. 4(e), we must take into account that

$$\frac{G}{G_0} = \frac{\rho_s/\rho_s^0 + C_b}{1 + C_b}. \tag{10}$$

It can be readily shown that $B_e = (1 + C_b)B$. The fact that $\rho_s \geqslant 0$ for the minimum G observed, $G_{\min}/G_0 = 0.8$ (see Fig. 4), implies that $C_b/(1 + C_b) < 0.8$, which leads to the upper bound of ∼4 for C_b. The corresponding theoretical value of $B = 0.503$ for the NCA method is obtained for $R = 0.27$ (Table I). Previously, a lower bound of 0.1 was estimated for Co on Cu(111) based on the quantum mirage effect assuming $C_b = 1$ [33]. For a more realistic value of the minimum ρ_s of about 60% of ρ_s^0 (the value for a surface without scattering sources), we obtain $B = 1.269$ and $R = 1$ (Table I), i.e., the same coupling of the impurity to the surface states as to the bulk ones.

VII. CONCLUSIONS

By combining STS and atomic lateral manipulation and applying a suitable Anderson Hamiltonian for the system, we have demonstrated that surface states have a relevant contribution in the formation of the Kondo state of Co/Ag(111). This result can be extended to other noble-metal surfaces and provides an important clue in the understanding of more complex correlated electron systems. The sensitivity of T_K to the surface state suggests the possibility to tune the coupling strength between a magnetic impurity and its closest environment using confining nanostructures with size comparable to λ_F [28]. In the case of Co/Ag(111) we provide a lower bound for the coupling of surface states to Co $3d$ states that is 27 % of the one to bulk states. Furthermore, we show that a two-channel SU(4) Anderson model (considering both spin and orbital quantum numbers) is more appropriate to describe the Kondo effect than the one-channel SU(2) model. We also show that the proximity of the onset of the surface state to the Fermi level plays a crucial role in the observed approximately linear dependence of the Kondo temperature on the surface density of states.

ACKNOWLEDGMENTS

We thank N. Lorente and R. Robles for fruitful discussions. We acknowledge financial support provided by the Spanish MINECO (Grants No. MAT2013-46593-C6-3-P and No. MAT2016-78293-C6-6-R), as well as the Argentinian CONICET (PIP 112-201101-00832) and ANPCyT (PICT 2013-1045). M.M.-L., D.S., and M.R.I. acknowledge the use of Servicio de Apoyo a la Investigación-Universidad de Zaragoza.

[1] J. Kondo, Prog. Theor. Phys. **32**, 37 (1964).
[2] V. Madhavan, W. Chen, T. Jamneala, M. F. Crommie, and N. S. Wingreen, Phys. Rev. B **64**, 165412 (2001).
[3] N. Knorr, M. A. Schneider, L. Diekhöner, P. Wahl, and K. Kern, Phys. Rev. Lett. **88**, 096804 (2002).
[4] L. Kouwenhoven and L. Glazman, Phys. World **14**, 33 (2001).
[5] J. Henzl and K. Morgenstern, Phys. Rev. Lett. **98**, 266601 (2007).
[6] K. Franke, G. Schulze, and J. Pascual, Science **332**, 940 (2011).
[7] A. Spinelli, M. Gerrits, R. Toskovic, B. Bryant, M. Ternes, and A. Otte, Nat. Commun. **6**, 10046 (2015).
[8] M. C. Martínez-Velarte, B. Kretz, M. Moro-Lagares, M. H. Aguirre, T. M. Riedemann, T. A. Lograsso, L. Morellon, M. R. Ibarra, A. Garcia-Lekue, and D. Serrate, Nano Lett. **17**, 4047 (2017).
[9] L. Cornils, A. Kamlapure, L. Zhou, S. Pradhan, A. A. Khajetoorians, J. Fransson, J. Wiebe, and R. Wiesendanger, Phys. Rev. Lett. **119**, 197002 (2017).
[10] J. Kondo, Phys. Rev. **169**, 437 (1968).
[11] A. C. Hewson, *The Kondo Problem to Heavy Fermions* (Cambridge University Press, Cambridge, UK, 1997).
[12] K. Andres, J. E. Graebner, and H. R. Ott, Phys. Rev. Lett. **35**, 1779 (1975).
[13] G. Aeppli and Z. Fisk, Comments Condens. Matter Phys. **16**, 1192 (1992).
[14] N. Roch, S. Florens, V. Bouchiat, W. Wernsdorfer, and F. Balestro, Nature (London) **453**, 633 (2008).
[15] J. J. Parks, A. R. Champagne, T. A. Costi, W. W. Shum, A. N. Pasupathy, E. Neuscamman, S. Flores-Torres, P. S. Cornaglia, A. A. Aligia, C. A. Balseiro *et al.*, Science **328**, 1370 (2010).
[16] S. Florens, A. Freyn, N. Roch, W. Wernsdorfer, F. Balestro, P. Roura-Bas, and A. Aligia, J. Phys.: Condens. Matter **23**, 243202 (2011).
[17] R. Vincent, S. Klyatskaya, M. Ruben, W. Wernsdorfer, and F. Balestro, Nature (London) **488**, 357 (2012).
[18] J. Li, W.-D. Schneider, R. Berndt, and B. Delley, Phys. Rev. Lett. **80**, 2893 (1998).
[19] V. Madhavan, W. Chen, T. Jamneala, M. F. Crommie, and N. S. Wingreen, Science **280**, 567 (1998).
[20] H. C. Manoharan, C. P. Lutz, and D. M. Eigler, Nature (London) **403**, 512 (2000).
[21] L. Limot, E. Pehlke, J. Kröger, and R. Berndt, Phys. Rev. Lett. **94**, 036805 (2005).
[22] D. Serrate, M. Moro-Lagares, M. Piantek, J. I. Pascual, and M. R. Ibarra, J. Phys. Chem. C **118**, 5827 (2014).
[23] A. Zhao, Q. Li, L. Chen, H. Xiang, W. Wang, S. Pan, B. Wang, X. Xiao, J. Yang, J. G. Hou *et al.*, Science **309**, 1542 (2005).
[24] T. Komeda, H. Isshiki, J. Liu, Y.-F. Zhang, N. Lorente, K. Katoh, B. K. Breedlove, and M. Yamashita, Nat. Commun. **2**, 217 (2011).
[25] E. Minamitani, N. Tsukahara, D. Matsunaka, Y. Kim, N. Takagi, and M. Kawai, Phys. Rev. Lett. **109**, 086602 (2012).
[26] V. Iancu, K. Schouteden, Z. Li, and C. Van Haesendonck, Chem. Commun. **52**, 11359 (2016).
[27] M. Ormaza, P. Abufager, B. Verlhac, N. Bachellier, M.-L. Bocquet, N. Lorente, and L. Limot, Nat. Commun. **8**, 1974 (2017).
[28] J. Fernández, M. Moro-Lagares, D. Serrate, and A. A. Aligia, Phys. Rev. B **94**, 075408 (2016).
[29] O. Újsághy, J. Kroha, L. Szunyogh, and A. Zawadowski, Phys. Rev. Lett. **85**, 2557 (2000).
[30] M. Plihal and J. W. Gadzuk, Phys. Rev. B **63**, 085404 (2001).
[31] M. A. Schneider, P. Wahl, L. Diekhöner, L. Vitali, G. Wittich, and K. Kern, Jpn. J. Appl. Phys. **44**, 5328 (2005).
[32] J. Merino and O. Gunnarsson, Phys. Rev. Lett. **93**, 156601 (2004).
[33] A. A. Aligia and A. M. Lobos, J. Phys.: Condens. Matter **17**, S1095 (2005).
[34] Q. Li, S. Yamazaki, T. Eguchi, H. Kim, S.-J. Kahng, J. F. Jia, Q. K. Xue, and Y. Hasegawa, Phys. Rev. B **80**, 115431 (2009).
[35] Q. L. Li, C. Zheng, R. Wang, B. F. Miao, R. X. Cao, L. Sun, D. Wu, Y. Z. Wu, S. C. Li, B. G. Wang *et al.*, Phys. Rev. B **97**, 035417 (2018).
[36] C.-Y. Lin, A. H. Castro Neto, and B. A. Jones, Phys. Rev. B **71**, 035417 (2005).
[37] M. Ternes, C. P. Lutz, C. F. Hirjibehedin, F. J. Giessibl, and A. J. Heinrich, Science **319**, 1066 (2008).
[38] A. A. Aligia, Phys. Rev. B **88**, 075128 (2013).
[39] In our own experiments as well as those of Ref. [35] the dip in the differential conductance has a considerable shift to the right of the Fermi level. This is consistent with a Kondo effect with total d occupancy n_d near 1 for SU(4) symmetry but is not consistent with either $n_d \approx 1$ and SU(2) symmetry or $n_d \approx 2$ for the two-channel model. In these two cases, the Kondo peak is practically at the Fermi level in the Kondo limit [67]. In the Supplemental Material of Ref. [35] the Friedel sum rule [67] is inverted to estimate $0.4 < n_d < 0.66$ based on the simplest one-channel SU(2) Anderson model. This would indicate that the system is in the intermediate valence regime, instead of the Kondo one. The same analysis for the SU(4) case gives $0.8 < n_d < 1.3$, which is fully consistent with our SU(4) model in the Kondo regime.
[40] M. Barral, S. Di Napoli, G. Blesio, P. Roura-Bas, A. Camjayi, L. Manuel, and A. Aligia, J. Chem. Phys. **146**, 092315 (2017).
[41] Calculations in a similar model indicate that the main effect of a finite U is a shift to lower energies of the Kondo dip and an increase of its width that can be absorbed by renormalizing the (unknown) magnitude of both surface and bulk hybridizations by the same factor [69].
[42] J. Li, W.-D. Schneider, and R. Berndt, Phys. Rev. B **56**, 7656 (1997)
[43] N. Bickers, Rev. Mod. Phys. **59**, 845 (1987).
[44] P. Anderson, J. Phys. C **3**, 2436 (1970).
[45] R. Žitko, Phys. Rev. B **84**, 085142 (2011).
[46] L. Vaugier, A. A. Aligia, and A. M. Lobos, Phys. Rev. B **76**, 165112 (2007).
[47] R. Žitko, Phys. Rev. B **84**, 195116 (2011).
[48] A. A. Aligia, P. Roura-Bas, and S. Florens, Phys. Rev. B **92**, 035404 (2015).
[49] J. Fernández, F. Lisandrini, P. Roura-Bas, C. Gazza, and A. A. Aligia, Phys. Rev. B **97**, 045144 (2018).
[50] T. Pruschke and N. Grewe, Z. Phys. B **74**, 439 (1989).
[51] D. E. Logan, M. P. Eastwood, and M. A. Tusch, J. Phys.: Condens. Matter **10**, 2673 (1998).
[52] J. Könemann, B. Kubala, J. König, and R. J. Haug, Phys. Rev. B **73**, 033313 (2006).
[53] J. Kroha and P. Wölfle, Acta Phys. Pol. B **29**, 3781 (1998).
[54] J. Fernández, A. A. Aligia, P. Roura-Bas, and J. A. Andrade, Phys. Rev. B **95**, 045143 (2017).
[55] N. S. Wingreen and Y. Meir, Phys. Rev. B **49**, 11040 (1994).

[56] F. Reinert, D. Ehm, S. Schmidt, G. Nicolay, S. Hüfner, J. Kroha, O. Trovarelli, and C. Geibel, Phys. Rev. Lett. **87**, 106401 (2001).
[57] D. Ehm, S. Hüfner, F. Reinert, J. Kroha, P. Wölfle, O. Stockert, C. Geibel, and H. v. Löhneysen, Phys. Rev. B **76**, 045117 (2007).
[58] L. Tosi, P. Roura-Bas, and A. Aligia, J. Phys.: Condens. Matter **27**, 335601 (2015).
[59] S. Di Napoli, P. Roura-Bas, A. Weichselbaum, and A. A. Aligia, Phys. Rev. B **90**, 125149 (2014).
[60] P. Roura Bas and A. A. Aligia, Phys. Rev. B **80**, 035308 (2009).
[61] P. Roura-Bas and A. A. Aligia, J. Phys.: Condens. Matter **22**, 025602 (2009).
[62] K. Haule, S. Kirchner, J. Kroha, and P. Wölfle, Phys. Rev. B **64**, 155111 (2001).
[63] L. Tosi, P. Roura-Bas, A. M. Llois, and L. O. Manuel, Phys. Rev. B **83**, 073301 (2011).
[64] M. A. Schneider, L. Vitali, N. Knorr, and K. Kern, Phys. Rev. B **65**, 121406 (2002).
[65] K. Nagaoka, T. Jamneala, M. Grobis, and M. F. Crommie, Phys. Rev. Lett. **88**, 077205 (2002).
[66] M. Moro-Lagares, *Engineering Spin Structures at the Atomic Scale* (Prensas de la Universidad de Zaragoza, Zaragoza, Spain, 2017).
[67] L. Tosi, P. Roura-Bas, A. Llois, and A. Aligia, Phys. B (Amsterdam, Neth.) **407**, 3263 (2012).
[68] Y.-F. Yang, Z. Fisk, H.-O. Lee, J. Thompson, and D. Pines, Nature (London) **454**, 611 (2008).
[69] J. Fernández, A. A. Aligia, and A. M. Lobos, Europhys. Lett. **109**, 37011 (2015).